NUMERICAL MODELLING OF A GEOSYNTHETIC REINFORCED STEEP SLOPE SUBJECTED TO SEISMIC LOADING

Castorina S. Vieira[1], M. Lurdes Lopes [1], and Laura Caldeira [2]

[1] University of Porto – Faculty of Engineering
R. Dr Roberto Frias, s/n 4200-465 Porto, Portugal
cvieira@fe.up.pt; lcosta@fe.up.pt

[2] National Laboratory of Civil Engineering
Av. do Brasil, 101, 1700-066 Lisbon, Portugal
laurac@lnec.pt

Keywords: Reinforced soil, Geosynthetics, Numerical modelling, Seismic loading.

Abstract. *In recent earthquakes the performance of reinforced soil retaining walls was diverse. The Hyogoken-Nambu (Kobe) Earthquake caused serious damage to conventional masonry retaining walls, unreinforced concrete gravity-type retaining walls and cantilever-type steel-reinforced concrete retaining walls, while geogrid-reinforced soil retaining walls, having a full-height concrete facing, performed very well during the earthquake [1]. On the other hand, the Chi-Chi earthquake, in Taiwan, caused serious damage to reinforced-soil retaining walls using keystones as facing [2].*

In this work the two-dimensional finite difference program Fast Lagrangian Analysis of Continua FLAC [3] was used to model the seismic response of a geogrid reinforced steep slope constructed in the North of Portugal. This structure was built in the Portuguese main itinerary, IP3, and is part of a reestablishment. The reinforced slope has an extension of about 206.2 m and the reinforced soil area reaches a maximum height of about 19.6 m. The slope behaviour was observed during 13 months, which includes three months of construction period.

The analysis of monitoring information of this geogrid reinforced steep slope and the numerical simulation of its construction are briefly presented. The seismic behaviour of this structure is analysed using FLAC program. Earthquake ground motions artificially generated with the program SIMQKE [4] were considered as seismic loading. The permanent displacements and reinforcement tensile forces are analysed and compared.

The numerical simulation of seismic loading showed a good performance of the reinforced steep slope. Since the structure is an overpass embankment, permanent vertical settlements can be the most disquieting factor. The residual reinforcement tensile forces remain smaller than the long term design strength of the geogrids.

1 INTRODUCTION

In recent earthquakes the performance of reinforced soil retaining walls was diverse. The Hyogoken-Nambu (Kobe) Earthquake caused serious damage to conventional masonry retaining walls, unreinforced concrete gravity-type retaining walls and cantilever-type steel-reinforced concrete retaining walls, while geogrid-reinforced soil retaining walls, having a full-height concrete facing, performed very well during the earthquake [1]. On the other hand, the Chi-Chi earthquake, in Taiwan, caused serious damage to reinforced-soil retaining walls using keystones as facing [2].

Usually reinforced soil retaining walls are designed using limit-equilibrium pseudo static methods. These methods are dependent only on peak ground acceleration, and disregard the effects due to duration of seismic action, frequency, foundation condition, stiffness of the reinforcement, facing type and others factors.

In this work the two-dimensional finite difference program *Fast Lagrangian Analysis of Continua* - FLAC [3] was used to investigate the seismic response of a geosynthetic reinforced steep slope. This code, suitable for modelling large distortions and dynamic response of earth structures, has also been used to investigate seismic response of reinforced soil retaining walls by other authors [5, 6].

2 BRIEF DESCRIPTION OF FLAC CODE AND SEISMIC LOADING

FLAC is an explicit finite difference program that performs a Lagrangian analysis. The finite difference method is perhaps the oldest numerical technique used for the solution of sets of differential equations, given initial values and/or boundary values [3]. For dynamic analyses the full equations of motion are solved using lumped gridpoint masses derived from the real density of surrounding zones (rather than fictitious masses used for static solution). Each triangular sub-zone contributes one-third of its mass (computed from zone density and area) to each of the three associated gridpoints. The final gridpoint mass is then divided by two in the case of a quadrilateral zone that contains two overlays. In finite-element terminology, FLAC uses lumped masses and a diagonal mass matrix [3].

In FLAC, the dynamic input can be applied as an acceleration history, as a velocity history, as a stress (or pressure) history or as a force history. Dynamic input can be applied either in the x or y directions corresponding to the xy axes for the model, or in the normal and shear directions to the model boundary.

Figure 1(a) presents one of the earthquake ground motions artificially generated [2] according to Portuguese National Annexes (PNA) of Eurocode 8 [7] for the greatest seismicity area of Portugal, considering seismic action type 2 (earthquake with moderate magnitude and small focal distance – close earthquake) and ground type B (deposits of very dense sand, gravel or very stiff clay). According to the PNA of Eurocode 8 [7], for the greatest seismicity area, the peak ground acceleration on type B ground is 2.5m/s^2 and 1.7 m/s^2 for seismic action type 2 and type 1, respectively. The duration of the stationary part of the accelerograms are equal to 10 seconds and 30 seconds. The Fourier spectrum for the accelerogram presented in Figure 1(a) is plotted in Figure 1(b).

Figure 2 shows the horizontal displacements obtained by double integration of the earthquake ground motion presented in Figure 1(a). Without correction, significant residual displacements occur at the end of the motion. To avoid these unreal large displacements at the end of the dynamic action, a baseline correction should be performed. A low frequency wave is determined which, when added to the original history, produces a final displacement equal

to zero (Figure 2). The velocity and acceleration time histories with and without baseline correction remain similar.
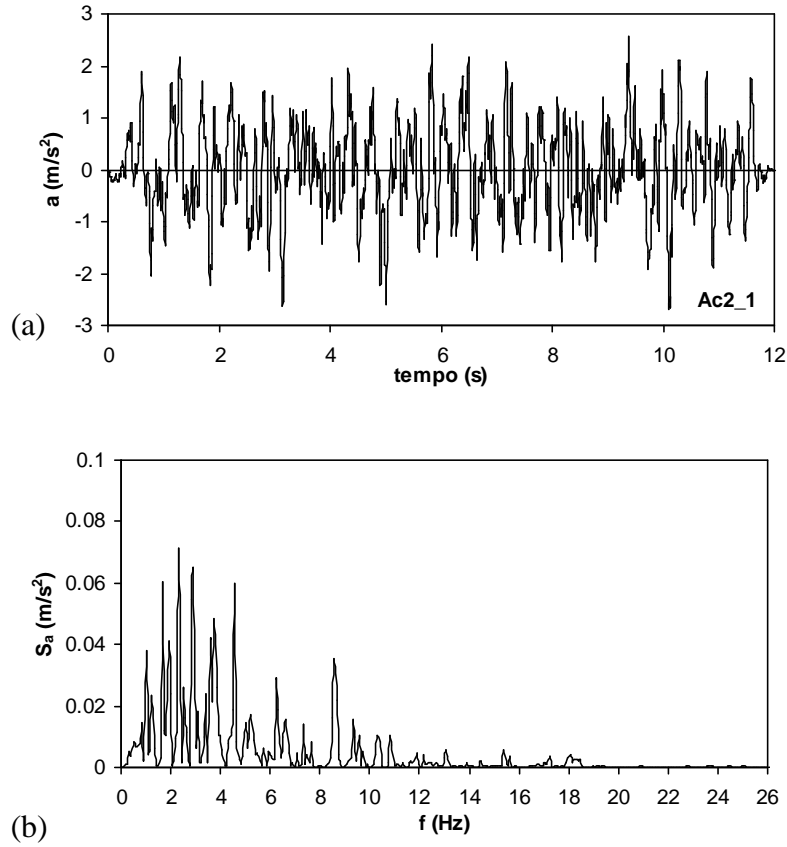

Figure 1: Example of one seismic action (type 2): a) artificial accelerogram [4]; b) Fourier spectrum.
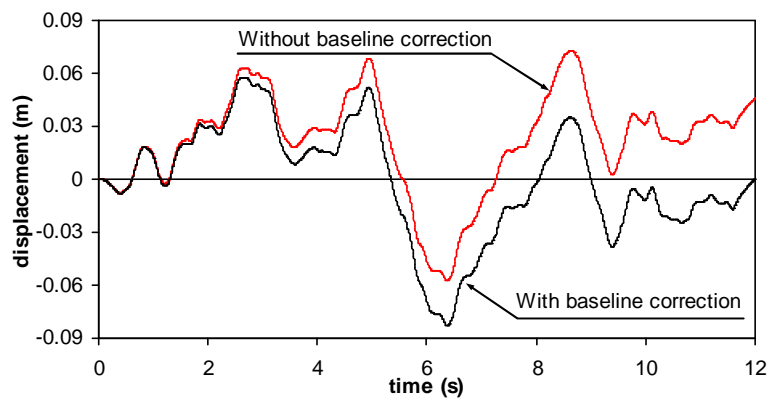

Figure 2: Effect of baseline correction on the imposed displacements.

To analyse the behaviour of this reinforced steep slope, earthquake ground motions artificially generated with the program SIMQKE [4] were considered as seismic loading. Two

types of seismic action were considered: an earthquake with moderate magnitude and small focal distance - "close" earthquake (seismic action type 2) and an earthquake with greater magnitude and greater focal distance – "distant" earthquake (seismic action type 1). Although the embankment was constructed in the lower seismicity area (North of Portugal), the most adverse scenery in terms of seismicity was considered. Ten accelerograms were analysed for each seismic action type.

3   GENERAL OVERVIEW OF THE STRUCTURE

The geogrid-reinforced steep slope was built (in 1998) in the Portuguese main itinerary (IP3) and is part of a reestablishment. The embankment has an extension of about 206.2 m and the reinforced soil area reaches a maximum height of about 19.6 m. On sections higher than 10 m, a bench with variable width parallel to the road pavement was built. The inclination of the reinforced slope is about 60º (Figure 3).

Figure 3: Overview of the embankment at the end of construction [8].

The foundation of the structure is a natural compact granite residual soil. Due to the local morphology, a rockfill was executed. The backfill is, also, a residual soil from granite. The reinforcements are high density polyethylene (HDPE) uniaxial geogrids, placed horizontally and spaced 0.60 m on vertical direction. In the analysed cross section, 31 layers of HDPE geogrids with nominal tensile strength of 160 kN/m (7 layers), 120 kN/m (10 layers), 90 kN/m (4 layers) and 60 kN/m (10 layers) were placed. The geogrids length is about 12.8m. The face units were constructed using welded wire net with quadrangular openings (Figure 4). A biodegradable mat was placed inside the face elements to prevent surface erosion and promote the vegetation growth (Figure 4b).

The reinforcement strains were measured in three reinforcement layers using linear extensometers spaced of 0.50 m (20 extensometers per monitored geogrid). Vertical stresses were recorded using load cells placed near the three monitorized geogrids. The internal horizontal displacements were recorded using two inclinometer tubes [8, 9]. The inclinometer I_1, also

called bench inclinometer, was placed at the middle of the bench width. The inclinometer I_2 was placed approximately at the middle of the higher bench (Figure 5). The displacements of the slope face were measured topographically. The analysed slope cross section, the monitoring devices and their positions are schematically represented in Figure 5.

The slope behaviour was observed during 13 months, which includes three months of construction period.

Figure 4: Detail of slope face: a) during the construction period [8]; b) August 2003 [9].
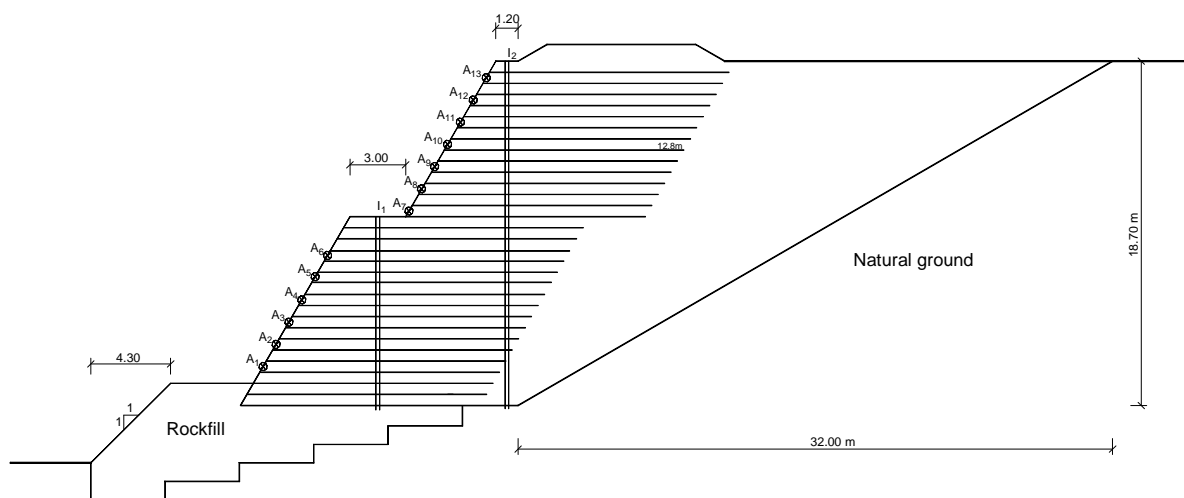
Figure 5: Analysed cross section and location of monitoring devices [9].

4 NUMERICAL MODELING OF THE CONSTRUCTION

4.1 Details of numerical modelling

The construction of an embankment is a progressive placement of soil layers. Consequently, the monitoring results are relative values. So, in order to compare the monitoring results with those obtained by the numerical analyses, the knowledge of the construction

sequence is imperative. An estimate was made, based on data from the instrumentation and some photographs found in [8, 10].

The fill was modelled as a purely frictional elasto-plastic material, with a Mohr-Coulomb yield function and a non-associated flow rule. The friction angle of the soil was taken equal to 35° and the unit weight $\gamma = 21.5$ kN/m^3. Young modulus and Poisson ratio of the soil were taken equal to 30 MPa and 0.3, respectively. After conducting a parametric study [9], it was considered a value of 5 kPa for the soil cohesion. This value has not a great physical significance but improves the performance of the numerical model, eliminating some numerical instability, particularly in the slope face.

The reinforcement layers were modelled using linear elasto-plastic cable elements with negligible compressive strength. The linear elastic stiffness of the reinforcement layers depends on the reinforcement strength and strain level. So, it was considered the value for 2% of geogrids strain. The interface between the reinforcement and the soil was modelled by a grout material [3] with an interface friction angle of 19.5° and a bond stiffness of 3×10^3 kN/m/m. These values were achieved from the numerical simulation of an in-situ pullout test [9].

The wrap-around face was modelled with cable elements with compressive strength not null (equal to 20% of reinforcement tensile strength) and an interface friction angle equal to 35°.

After the clearing of natural ground, it was decided [8] to place a rockfill under and in front of the reinforced soil mass (see Figure 5). The foundation and the rockfill were modelled as elastic materials with Young modulus of 200 MPa. Over the rockfill foundation, it was considered a thin layer of soil, with similar properties to those of the backfill, which is the base for the first reinforcement layer.

In order to model, as closely as possible, the real construction sequence, the embankment was simulated by the placement of successive soil layers of 0.30 m thick. The pavement was simulated by a layer with increased density. When the position of the reinforcement layer "i" is achieved, the horizontal displacement of the face at this level is prevented, being allowed only in the next stage, ie the reinforcement layer "i" is only loaded in the following construction stage.

4.2 Comparison of numerical results with monitoring data

Taking into account the reference values of the topographic targets and the construction sequence, intermediate measurements of the face displacements were performed in the numerical analyses. With these intermediate values it was possible to obtain relative displacements comparable with those obtained with monitoring. To make possible the comparison between the internal displacements of the embankment obtained with the numerical analyses and the values recorded in the inclinometer tubes, intermediate measurements of the horizontal displacements along two vertical planes (coincident with the inclinometer tubes position - see Figure 5) were also performed.

Figure 6 compares the relative displacements of the slope face achieved in the numerical analyses with those from the topographic measurements. The analysis of this figure shows that the numerical model captures the real behaviour of the reinforced embankment. In the four targets placed nearest the top, the horizontal displacements of the model are very close to values recorded in-situ. In the remaining targets, the numerical model tends to overestimate the horizontal displacements of the slope face. The model reproduced very closely the vertical displacements of the slope face. Note that the targets were fixed to the welded wire net, which means, their movements may be related to a punctual displacement of the wire net and not to

the behaviour of slope face. The numerical modelling of the real conditions of the slope face is not easy, since the system face is complex (geogrid+ biodegradable mat+ welded wire net).
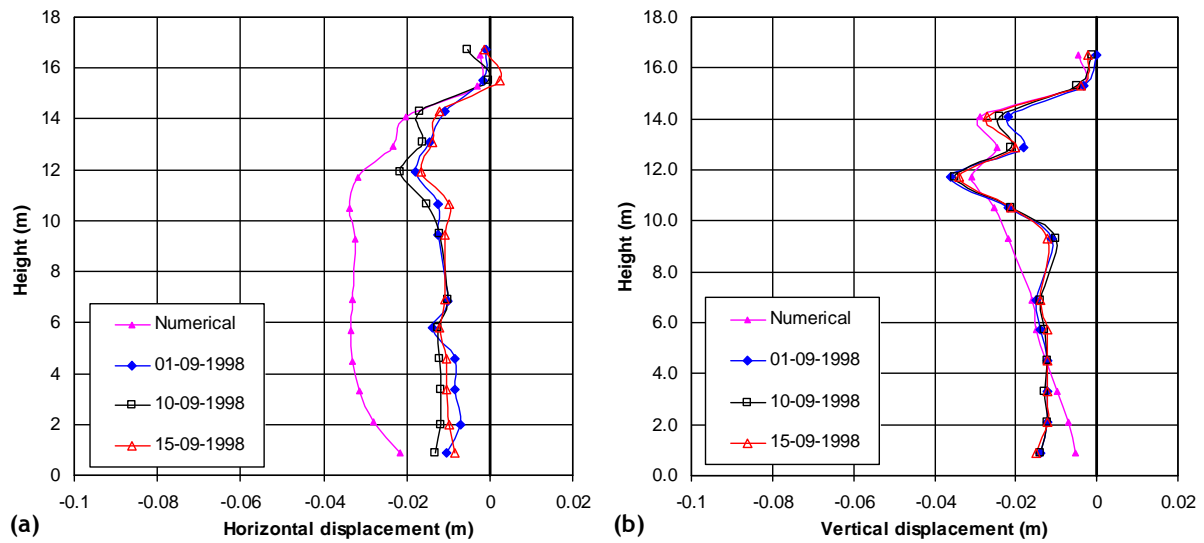

Figure 6: Comparison of numerical and monitoring results: a) horizontal displacements of the slope face; b) vertical displacements of the slope face.

Figure 7 presents the internal horizontal displacements along two vertical planes coincident with the inclinometer tubes position. The numerical results are compared with those obtained from the monitoring.

Figure 7 shows that the numerical analysis seems suitable for the internal horizontal displacements, particularly those relating to the inclinometer I_2 (Figure 7b). For the bench inclinometer (or inclinometer I_1), located near the slope face, the numerical analysis did not show the same effectiveness. For this inclinometer, the numerical model tends to overestimate the internal displacements in the upper part of the inclinometer. This may be partly justified by the influence of the complex face system.
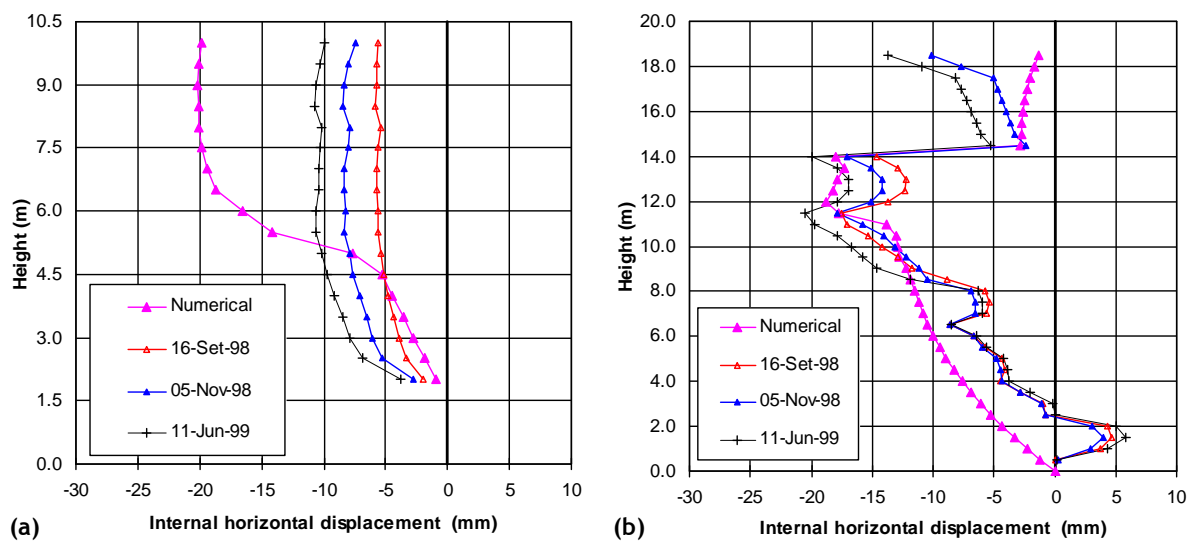

Figure 7: Comparison of internal horizontal displacements reached with numerical analyses and monitoring results: a) inclinometer I_1; b) inclinometer I_2.

7

5   SEISMIC BEHAVIOUR OF THE STRUCTURE

5.1   General

As mentioned, two types of seismic action were considered: an earthquake with moderate magnitude and small focal distance - "close" earthquake (seismic action type 2) and an earthquake with greater magnitude and greater focal distance - "distant" earthquake (seismic action type 1). In order to select 10 accelerograms representative of seismic action type 2 and 10 accelerograms representative of seismic action type 1, several series were artificially generated. Time increments of 0.01 seconds were considered. For seismic action type 2 and type 1, the duration of the stationary part of the accelerograms are equal to 10 seconds and 30s seconds and the duration of the transitory sections, before and after the stationary part, are equal to 1 second and 3 seconds, respectively.

To avoid the reflection of the waves back into the model, absorbing boundaries (free-field conditions [3]) were considered at the lateral limits of the mesh.

The hysteretic damping of the foundation and rockfill was represented by an equivalent Rayleigh damping with damping coefficient of 10%. In addition to the damping associated to the elasto-plastic behaviour of the backfill, no additional damping was considered.

5.2   Results for seismic action type 2 – "close" earthquake

Figure 8 presents time histories of horizontal displacements recorded at three points located at the slope face. The horizontal displacement at the base of reinforced slope (Point 1) follows closely the imposed displacement at the foundation. Note that, a rockfill was placed in front of the first reinforcement layers (up to 1.5 m high). The horizontal displacement at the crest of the upper slope (Point 3) in outside direction (negative values in Figure 8), tends to be smaller than those recorded at the crest of the lower slope (Point 2).

As an example, Figure 9 shows the geometry of the reinforced steep slope at the end of the seismic action Ac2_6. Note that the displacements were enlarged 10 times. It is evident some instability at the bench, including swelling of the soil. Vertical displacements with some significance are also shown at the top.

Figure 10 presents the reinforced load developed in a cable element of the 4th reinforcement layer. This element is located about 3 m from the slope face. The seismic horizontal displacement of one node of the same element is also plotted. In the time history of this reinforcement load, three sudden increases are visible. These increases occur when the accelerogram inverts the sign. In the horizontal displacement time history, positive values mean displacements inwards of reinforced slope.

Figure 11 shows the average curves of horizontal and vertical displacements of the slope face and those obtained by adding and subtracting the respective standard deviation, for the ten accelerograms considered (seismic action type 2). The analysis of this figure shows that, on the slope below the bench, the maximum horizontal displacement occurs in the upper half of the slope. In the slope above the bench the horizontal displacements in the upper half are lower. The maximum vertical displacement occurs at the crest of the embankment.

Figure 12 presents the average values of residual reinforcement tensile forces in all reinforcement layers and those obtained by adding and subtracting the respective standard deviation. To understand the sudden changes shown, it was included the reference to geogrids with distinct properties. Note that, geogrids with nominal strength of 160 kN/m and 120 kN/m
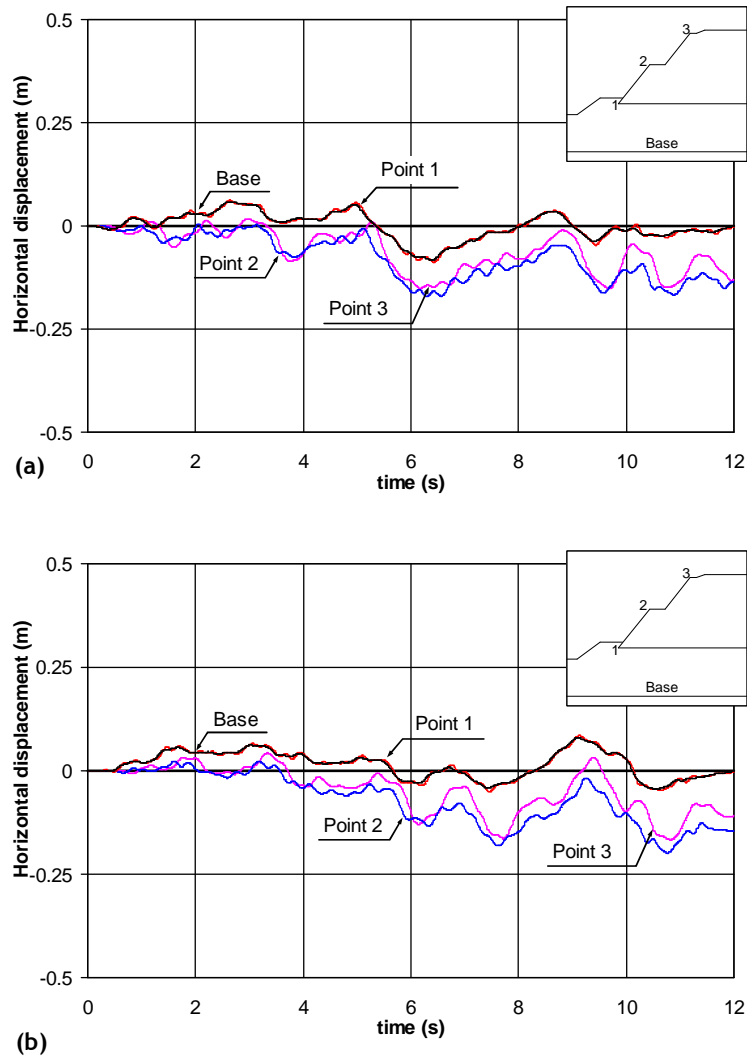
Figure 8: Horizontal displacements time histories of 3 points located at the slope face:
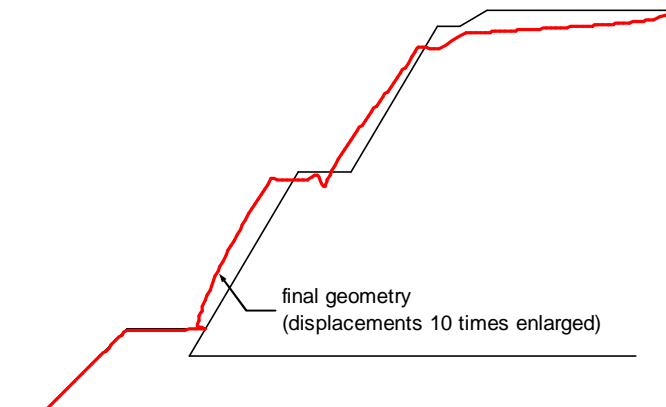a) accelerogram Ac2_1;.b) accelerogram Ac2_6.

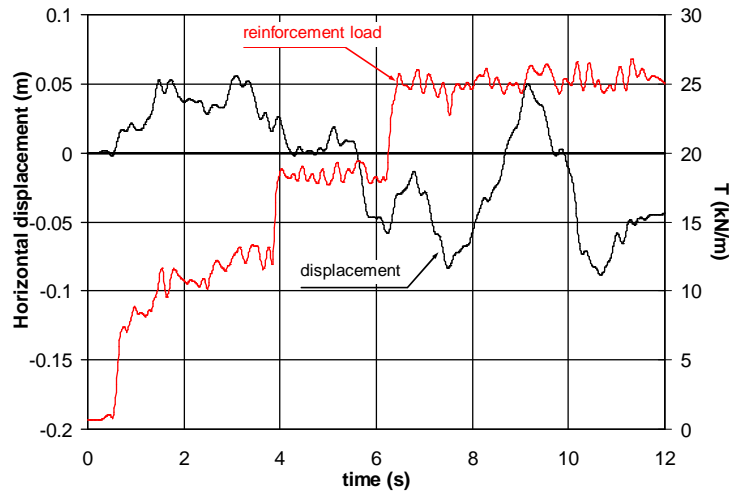Figure 9: Deformed slope at the end of seismic action Ac2_6.

Figure 10: Time histories of reinforcement load and horizontal displacement recorded in one element of the 4th geogrid level (Ac2_6).
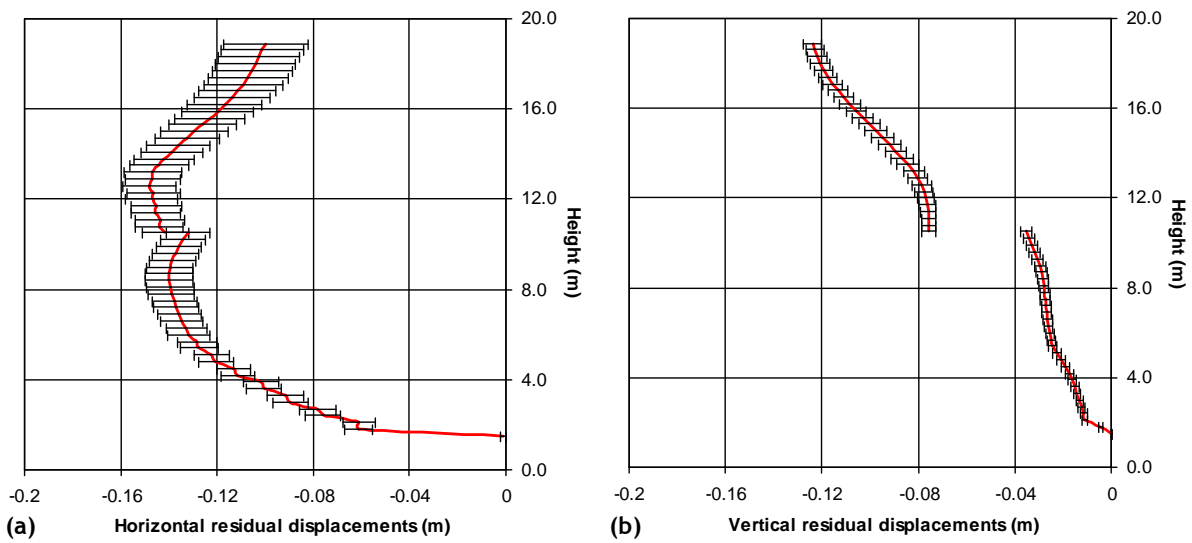
Figure 11: Pattern of mean residual displacements for seismic action Type 2: a) horizontal residual displacements of slope face; b) vertical residual displacements of slope face.

were placed on the embankment below the bench and geogrids with nominal strength of 90 kN/m and 60 kN/m were installed on the embankment above the bench. The presence of the rockfill in front of the lower reinforcement layers reduces, significantly, the tensile forces mobilized at these layers.

Although not presented in this work, it is important to mention that the maximum tensile loads recorded in the reinforcement elements located on the upper slope are very close to the residual values (at the end of motion). On the slope below the bench, the maximum tensile loads exceed the residual values, particularly in the 4th reinforcement layer (the first layer placed above the rockfill), where the difference can be substantial (around 50%).
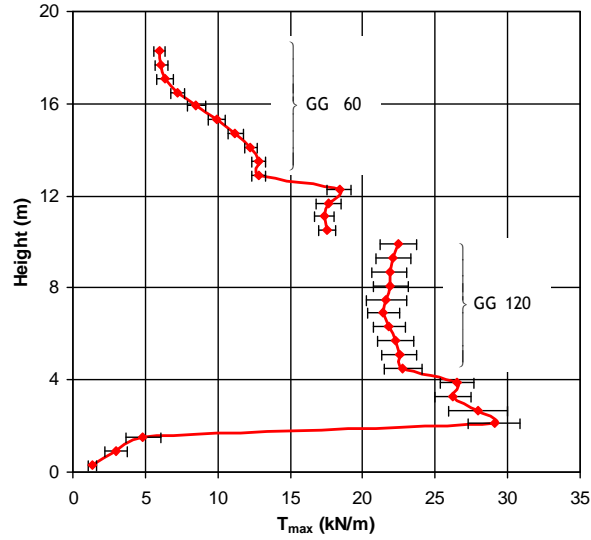
Figure 12: Pattern of mean residual reinforcement tensile forces for seismic action Type 2.

5.3 Results for seismic action type 1 – "distant" earthquake

Figure 13 shows time histories of horizontal displacements recorded at three points located at the slope face for the artificial accelerogram Ac1_9. As observed for the "close" earthquake, the horizontal displacement at the base of reinforced slope (Point 1) follows closely the imposed displacement at the foundation.

The horizontal displacements recorded during the simulated earthquakes are quite distinct (compare Figure 8 and Figure 13). Even so, the permanent horizontal displacements at the end of ground motion are not very different.
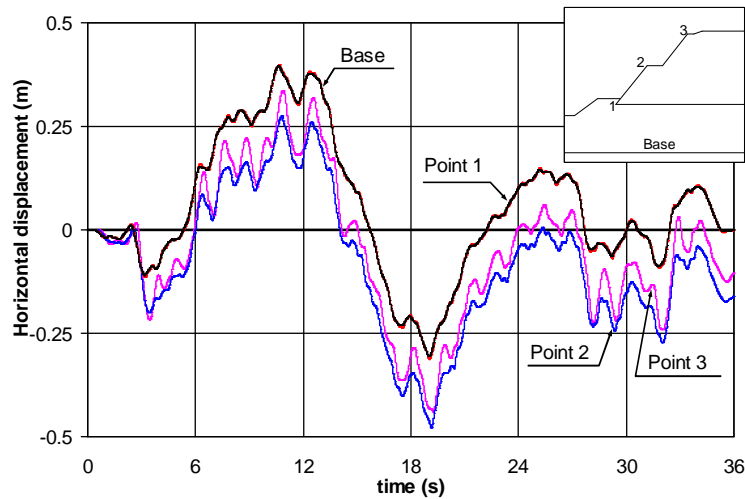

Figure 13: Horizontal displacements time histories of 3 points located at the slope face for the accelerogram Ac1_9.

Figure 14 illustrates the reinforced load recorded in a cable element of the 4th reinforcement layer during the numerical simulation relating to the accelerogram Ac1_9. The seismic

11

horizontal displacement of one node of the same element is also plotted. As noted for the seismic action type 2, the reinforcement load tends to experience sudden increases. Although, for the accelerograms representative of seismic action type 1, after some seconds, the changes in the reinforcement load are very small (Figure 14).
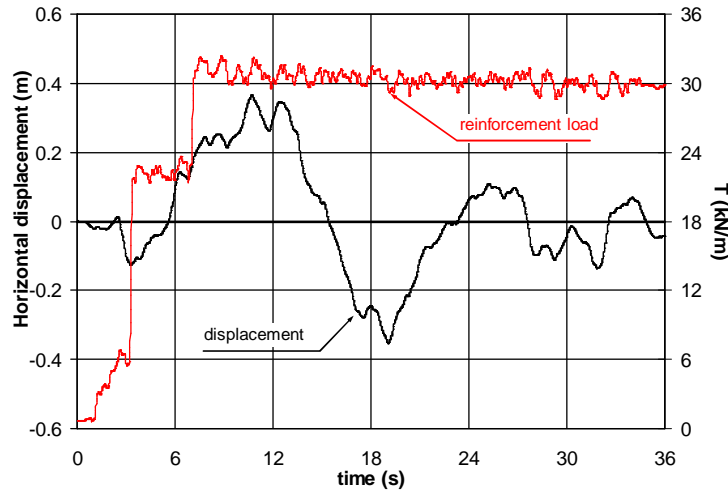

Figure 14: Time histories of reinforcement load and horizontal displacement recorded in one element of the 4th geogrid level (Ac1_9).

The average curves of horizontal and vertical displacements of the slope face, and those obtained by adding and subtracting the respective standard deviation, for the accelerograms representative of the seismic action type 1 are presented in Figure 15. As verified for the seismic action type 2 (Figure 11), the maximum horizontal displacements occur in the upper half of the slope below the bench and in the lower half of the slope above the bench. The maximum vertical displacement occurs at the crest of the embankment.
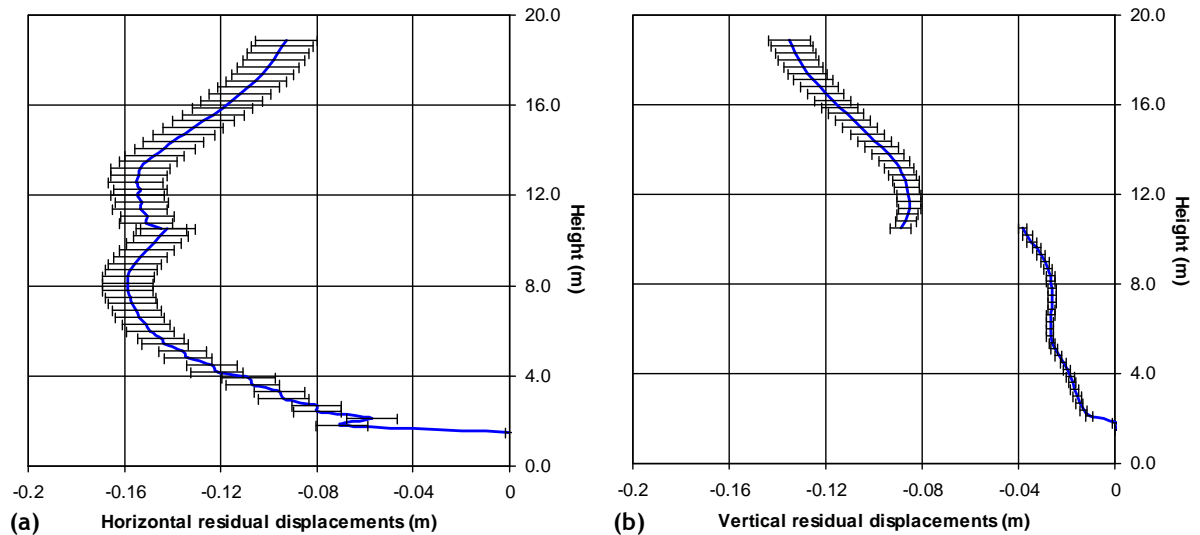

Figure 15: Pattern of mean residual displacements for seismic action Type 1: a) horizontal residual displacements of slope face; b) vertical residual displacements of slope face.

Figure 16 illustrates the average values of residual tensile forces in all reinforcement layers, and those obtained by adding and subtracting the respective standard deviation. The residual tensile forces distribution through the structure height is similar to that presented in Figure 12 for "close" earthquakes.
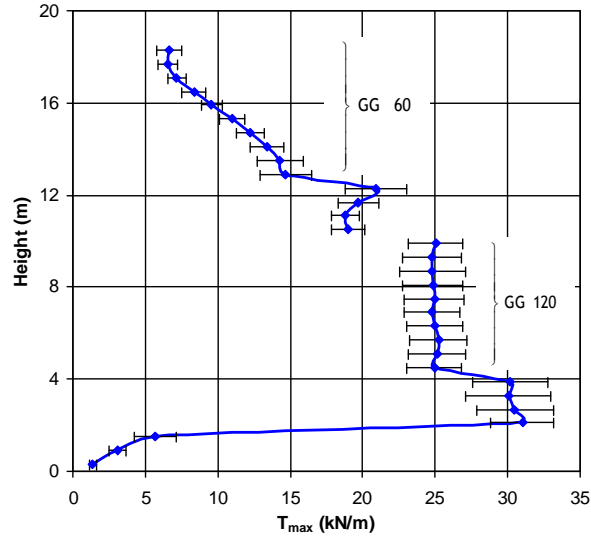

Figure 16: Pattern of mean residual reinforcement tensile forces for seismic action Type 1.

5.4 Influence of seismic action type

Figure 17 compares the average curves of horizontal and vertical displacements of the slope face for the two seismic actions considered. The first conclusion to be drawn, from the analysis of this figure, is that the "distant" earthquake is more adverse for the performance of this reinforced steep slope.
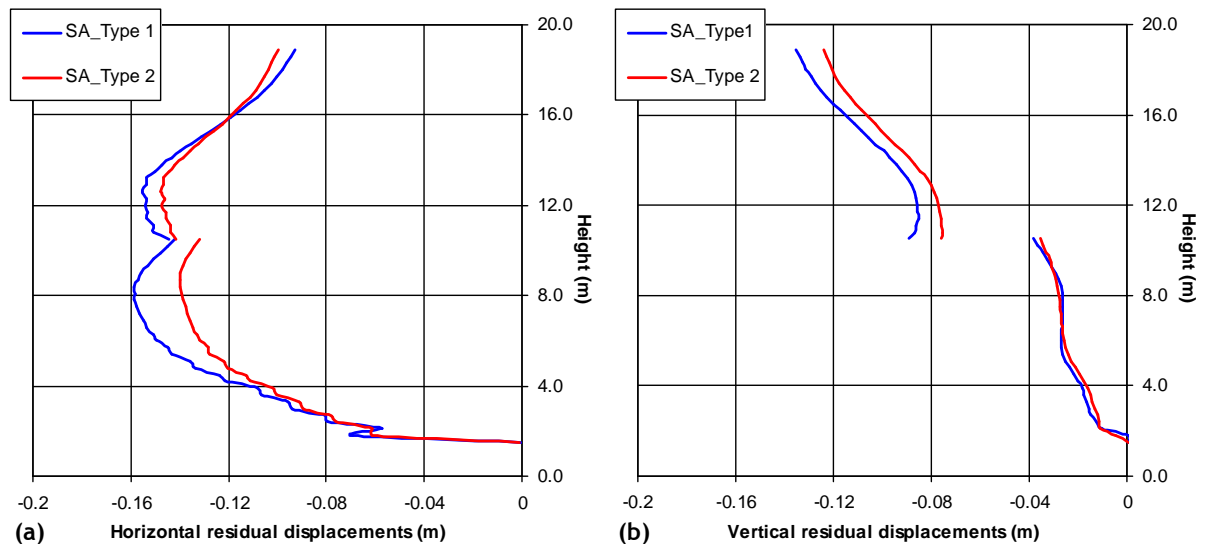

Figure 17: Influence of seismic action type on residual displacements of slope face: a) horizontal displacements; b) vertical displacements.

On average, the horizontal and vertical displacements recorded for "distant" earthquakes are, respectively, 7.1% and 9.1% greater than those recorded for "close" earthquakes. Even so,

13

the horizontal displacements of the slope face near the top tend to be lower when the structure is subjected to distant earthquakes. The vertical displacements of the slope below the bench are quite small and they are not influenced by the seismic action type.

Figure 18 illustrates the average values of maximum reinforcement tensile loads at the end of ground motion (residual values) for the two seismic actions. The distribution of residual reinforcement tensile loads trough the structure height is similar. However the seismic action type 1 generates greater reinforcement loads.

The maximum values of the residual reinforcement tensile loads remain smaller than the long term design strength of the geogrids. These latter values are, according to [8], 46.1 kN/m, 35.0 kN/m, 25.9 kN/m and 17.5 kN/m for the geogrids GG160, GG120, GG90 and GG60, respectively.
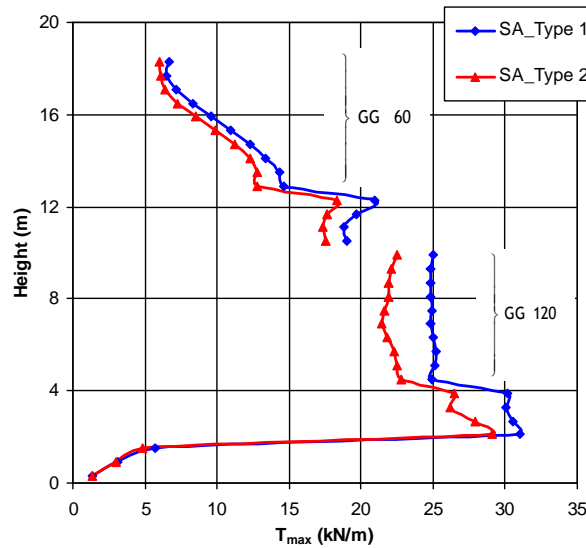

Figure 18: Influence of seismic action type on residual reinforcement tensile forces.

6   MAIN CONCLUSIONS

Despite some limitations related to the characterization and real progress of the embankment construction, resulting from the fact that the first author of this work did not follow the design and construction of the structure, the obtained results fit reasonably with the monitoring data. It was found that:

- with respect to distribution of slope face displacements through the structure height, either horizontal or vertical, the numerical model captures the real behaviour of the embankment;

- numerical modelling also seems appropriate for the internal horizontal displacements.

The numerical simulation of seismic loading showed a good performance of the reinforced steep slope. Since the structure is an overpass embankment, permanent vertical settlements can be the most disquieting factor. However, it should be noted that, according to the philosophy of safety codes, under the action of intense earthquakes, the occurrence of damages is allowed, provided they do not produce the rupture of the structure.

The residual reinforcement tensile forces remain smaller than the long term design strength of the geogrids.

The occurrence of a "distant" earthquake seems to be more adverse for the seismic performance of this structure. Nevertheless, numerical modelling of other geosynthetic reinforced soil structures has shown that "close" earthquakes can be critical. The fundamental frequencies of these structures will have, certainly, its influence.

ACKNOWLEDGMENTS

REFERENCES

[1]   Tatsuoka, F., Koseki, J., Tateyama, M., and Horii, K.(1995). Performance of soil retaining walls during the Great Hanshin-Awaji Earthquake. *Bulletin of Earthquake Resistant Structures Research Center, University of Tokyo,* (28), pp. 3-12.

[2]   Koseki, J. and Hayano, K.(2000). Preliminary Report on damage to retaining walls caused by the 1999 Chi-Chi earthquake. *Bulletin of Earthquake Resistant Structures Research Center, University of Tokyo,* (33), pp. 23-34.

[3]   Itasca (2005). FLAC - Fast Lagrangian Analysis of Continua, in *Version 5.00, Itasca Consulting Group, Inc., USA.*

[4]   Gasparini, D. and Vanmarcke, E. (1976). SIMQKE - A computer program for artificial motion generation, in *User's Manual and Documentation*, Department of Civil Engineering, Massachussets Institute of Technology.

[5]   Bathurst, R.J. and Hatami, K.(1998). Seismic response analysis of a geosynthetic-reinforced soil retaining wall. *Geosynthetics International,* 5(1-2), pp. 127-166.

[6]   El-Emam, M.M. (2003). Behaviour of reinforced soil walls under earthquake loading. PhD Thesis, Queen's University at Kingston, 411 p Behaviour of reinforced soil walls under earthquake loading.

[7]   NP-ENV 1998-1-1 (2000). Eurocode 8: Design provisions for earthquake resistance of structures. Part 1-1: General rules – Seismic actions and general requirements for structures. *Portuguese NAD*, pp. 34.

[8]   Lopes, M.L., Mendonça, A., Monteiro, B.P., Pais, M.J., and Caspurro, I.M. (1999). Geogrid reinforced embankment constructed in branch Régua-Reconcos of IP3 - Construction, in *Technical Report. Protocol JAE/FEUP (in Portuguese).*

[9]   Vieira, C.S. (2008). Geosynthetic reinforced soil retaining walls and slopes. Seismic behaviour and design methodologies. PhD Thesis, Civil Engineering Department, University of Porto, 575 p (in Portuguese).

[10]   Mendonça, A., Lopes, M.L., and Pinho Lopes, M.J.(2003). Construction and post-construction behaviour of a geogrid-reinforced steep slope. *Geotechnical and Geological Engineering,* 21, pp. 129–147.